Redox Biology 67 (2023) 102928

Contents lists available at ScienceDirect

Redox Biology

journal homepage: www.elsevier.com/locate/redox

# Nitric oxide inhibits FTO demethylase activity to regulate $N^6$-methyladenosine mRNA methylation

Hannah Petraitis Kuschman [a], Marianne B. Palczewski [a], Brian Hoffman [e], Mary Menhart [b], Xiaowei Wang [b], Sharon Glynn [d], Abul B.M.M.K. Islam [c], Elizaveta V. Benevolenskaya [c], Douglas D. Thomas [a,*]

[a] University of Illinois Chicago, College of Pharmacy, Department of Pharmaceutical Sciences, USA
[b] College of Medicine, Departments of Pharmacology and Bioengineering, USA
[c] Biochemistry and Molecular Genetics, USA
[d] University of Galway, College of Medicine, Nursing and Health Sciences, School of Medicine, D. of Pathology, USA
[e] Weinberg College of Arts and Sciences, Northwestern University, Department of Chemistry, USA

A B S T R A C T

$N^6$-methyladenosine ($m^6A$) is the most abundant internal modification on eukaryotic mRNAs. Demethylation of $m^6A$ on mRNA is catalyzed by the enzyme fat mass and obesity-associated protein (FTO), a member of the nonheme Fe(II) and 2-oxoglutarate (2-OG)-dependent family of dioxygenases. FTO activity and $m^6A$-mRNA are dysregulated in multiple diseases including cancers, yet endogenous signaling molecules that modulate FTO activity have not been identified. Here we show that nitric oxide (NO) is a potent inhibitor of FTO demethylase activity by directly binding to the catalytic iron center, which causes global $m^6A$ hypermethylation of mRNA in cells and results in gene-specific enrichment of $m^6A$ on mRNA of NO-regulated transcripts. Both cell culture and tumor xenograft models demonstrated that endogenous NO synthesis can regulate $m^6A$-mRNA levels and transcriptional changes of $m^6A$-associated genes. These results build a direct link between NO and $m^6A$-mRNA regulation and reveal a novel signaling mechanism of NO as an endogenous regulator of the epitranscriptome.

## 1. Introduction

Nitric oxide (NO) is an essential biological free radical that functions as a signaling molecule by either directly binding metal centers, such as the activation of soluble guanylate cyclase (sGC), or by forming nitrogen oxide-based covalent protein modifications (i.e. *S*-nitrosothiols (RSNO)) to mediate fundamental physiological processes including vasodilation, neurotransmission, and host defense [1–6]. Conversely, dysregulated NO production is associated with a range of pathological conditions, yet canonical NO signaling mechanisms cannot explain the vast number of transcriptional changes associated with NO-driven disease states [6,7]. For example, studies show that sGC activation cannot account for all NO-regulated gene expression changes [7] and that chronically elevated NO can lead to the inactivation and degradation of sGC [6]. Aberrant NO signaling is especially prominent in cancers where increased NO production, due to the induction of the inducible form of nitric oxide synthase (NOS2), is associated with tumor gene expression, poor patient outcome, increased mortality, and resistance to chemotherapy across diverse cancer types [2,8,9]; these include triple-negative breast (TNBC) [10–22], lung [23–25], prostate [26–28], brain [29,30], colon [31–33], melanoma [34–37], and liver cancers [38,39].

Epitranscriptomic processes are mediated through post-transcriptional modifications to RNA (i.e., $m^6A$), and are essential physiological determinants of mRNA metabolism and cell fate. $M^6A$-methylation on mRNA establishes and maintains transcriptional states by controlling mRNA splicing, transport, translation, and degradation [40,41]. $M^6A$ is a reversible modification on mRNA which is installed by methyltransferase complexes (such as METTL3–METTL14) [42] and oxidatively removed by mRNA demethylases FTO and alkB homolog 5 (ALKBH5) [43,44]. Steady-state levels of $m^6A$ on mRNA are maintained by the coordinated activities of the methyltransferases and demethylases. Despite the physiological importance of $m^6A$ in regulating the mRNA transcriptome, dysregulation of $m^6A$-mRNA is also associated with numerous pathological conditions [45–47]. For example, dysregulation of $m^6A$ on mRNA is related to the etiology and progression of numerous cancer types (breast, lung, prostate, liver, leukemia, brain, colon, etc.) as well as resistance to antitumor therapy [48–50]. Although there is a strong association of $m^6A$ with pathological cancer phenotypes, underlying mechanisms that establish tumor-permissive patterns of $m^6A$ in cancers have not been fully realized.

* Corresponding author.
*E-mail address:* ddthomas@uic.edu (D.D. Thomas).

https://doi.org/10.1016/j.redox.2023.102928
Received 31 August 2023; Received in revised form 27 September 2023; Accepted 7 October 2023
Available online 14 October 2023

As FTO plays an essential role in demethylating m$^6$A-mRNA, overall amounts of m$^6$A-mRNA are a partial reflection of FTO activity and can change dynamically. For example, m$^6$A-mRNA levels can be affected by the availability of endogenous FTO substrates and co-factors (Fe(II), ascorbate, $O_2$, 2-OG) or by the accumulation of oncometabolites, such as 2-hydroxyglutarate, which competitively inhibits FTO (a 2-OG-dependent enzyme) [51]. Identifying key endogenous signaling molecules that control FTO activity under physiological versus pathological conditions is fundamental to understanding how m$^6$A-mRNA dysregulation contributes to disease etiology and progression. As a member of the Fe(II)/2-OG-dependent family of enzymes, FTO contains a non-heme iron in its active site [52]. Binding of $O_2$ to this iron atom is a critical catalytic step in the demethylation reaction, and we hypothesized that NO would target this iron site because of NO's structural and bonding similarity to $O_2$. Here, we report that NO is an endogenously produced inhibitor of FTO m$^6$A-mRNA demethylase activity. We demonstrate that FTO loss-of-function (chemical inhibition or genetic knockdown) replicated the effects of NO on m$^6$A-mRNA levels and associated gene expression changes. We further found that a subset of mRNA transcripts were enriched with m$^6$A and were changed at steady-state levels in cancer cells chronically treated with NO and in NO-producing xenograft tumors. Changes in m$^6$A-mRNA could not be attributed to changes in methyltransferase activity or expression levels of mRNA-methyl-modifying enzymes. Collectively, these experiments establish NO as an endogenous regulator of the epitranscriptome, mediated by changes in m$^6$A-mRNA.

## 2. Results

### 2.1. Nitric oxide inhibits the catalytic activity of the RNA demethylase FTO by binding to the mononuclear non-heme iron atom

FTO directly demethylates m$^6$A on mRNA to unmethylated adenosine(A) and in the process converts 2-oxoglutarate (2OG, a cofactor) to succinate. To test whether NO could inhibit FTO catalytic activity, we incubated recombinant full-length FTO protein in the presence of all cofactors (2-OG, Fe(II), ascorbate) and substrate (synthetic RNA oligos containing a single m$^6$A-methylated base) and measured product formation (conversion of 2OG to succinate) in the presence of NO, using the NO-donor compound Sper/NO (Spermine NONOate, 5-3000 μM ≈ 500 nM–30 μM $[NO]_{SS}$, Fig. 1A). Next, we incubated recombinant full-length FTO protein with NO and measured the conversion of m$^6$A-mRNA to A-mRNA by ELISA (Fig. 1B). For both assays, NO significantly inhibited FTO activity with similar IC50s for the NO-donor Sper/NO. To test whether NO interacts with the iron center, we conducted electron paramagnetic resonance (EPR) studies of FTO treated with NO in the presence of all cofactors and substrates. EPR spectra showed that the enzyme does not accumulate the S = 3/2 mononitrosyl complex (Fe(II)–NO), with its intense $g_{\perp} \sim 4.1$ signal, and instead revealed the characteristic S = ½ signal of a non-heme dinitrosyl iron complex (DNIC, [Fe(NO)$_2$] [9]), with $g_{\perp} \sim 2.03$, $g_{||} \sim 2.01$ (Fig. 1C) [53,54]. The DNIC signal was not detected when the FTO enzyme was omitted from the complete reaction mixture, indicating that the observed DNIC signal is associated with the enzyme, and not with a complex formed in solution.

### 2.2. Human cancer cells exposed to NO exhibit global increases in m$^6$A in mRNA

To test whether NO could inhibit endogenous m$^6$A-mRNA demethylase activity, we studied 6 cell lines derived from 5 different human cancer types (breast, brain, ovarian, prostate, and lung) that are known to synthesize NO [55]. These cells were treated with low physiological levels of NO using the NO-donor DETA/NO ($t_{½}$ = 22 h), and after 24 h, significant increases in m$^6$A-mRNA were found in all cell lines (Fig. 2A). Dysregulated NO synthesis is associated with numerous cancers, and patients with triple negative breast cancer (TNBC) whose tumors produce NO have significantly increased mortality compared to TNBC patients whose tumors do not produce NO [55]. For subsequent experiments we focus on two TNBC cell lines (MDA-MB-231, MDA-MB-468). In TNBC cells, increases in m$^6$A-mRNA were concentration-dependent (Fig. 2B), and persisted during chronic NO exposure (10-days, Fig. 2C). To test whether m$^6$A-mRNA would be similarly increased in cells endogenously synthesizing NO, we transfected MDA-MD-231 cells with either a human inducible nitric oxide synthase (NOS2) gene or an empty vector control (VC) plasmid (Fig. 2D). After 72 h incubation, we measured both NO synthesis (stable NO-oxidation products (nitrite/nitrate) in the media) (Fig. 2E) and m$^6$A-mRNA (Fig. 2F). NO production was detected in the NOS2 transfected cells but not in the cells transfected with the empty vector plasmid or in the NOS2 cells treated with a pan-NOS inhibitor (L-NAME). Similarly, m$^6$A-mRNA was elevated only in the NO-producing cells but not the control cells or NOS2 cells treated with L-NAME.

To provide further evidence that NO-mediated increases in m$^6$A-mRNA were due to FTO inhibition, we compared the levels of m$^6$A-mRNA in cells treated with NO to cells either treated with a selective inhibitor of FTO (meclofenamic acid, MA) [56] or to cells where FTO protein was depleted. M$^6$A-mRNA significantly increased to a similar magnitude in both the MA-treated cells and in the NO-treated cells (Fig. 2G and H). When FTO was knocked down (Fig. 2I), m$^6$A-mRNA increased significantly at baseline compared to the control cells or cells

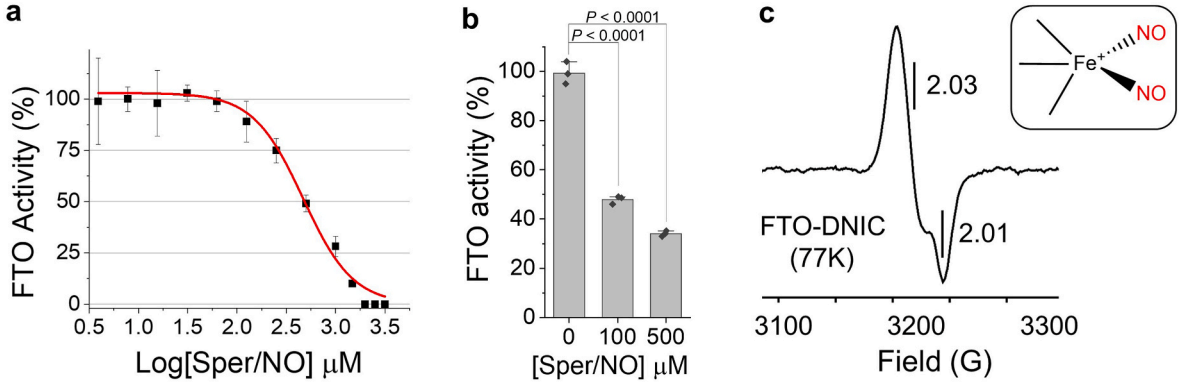


**Fig. 1. NO inhibits FTO demethylase activity by forming a DNIC.** FTO activity measurements using recombinant full-length FTO protein incubated for 90 min with a m$^6$A-RNA substrate and NO (Sper/NO) via **a**, detection of succinate production (representative graph with error bars is the mean ± s.d., data were independently replicated 3 times with similar results), and **b**, conversion of m$^6$A-mRNA to A-mRNA, at 3 h, ELISA (n = 3 separate reactions). Data are represented as mean ± s.e.m., *P*-values were determined by unpaired two-tailed Student's *t*-tests. **c**, Representative X-Band (77 K) EPR spectra of FTO and all cofactors and substrate treated with NO (DEA/NO, 25 μM) for 30 min (n = 3). Inset showing representative DNIC structure.

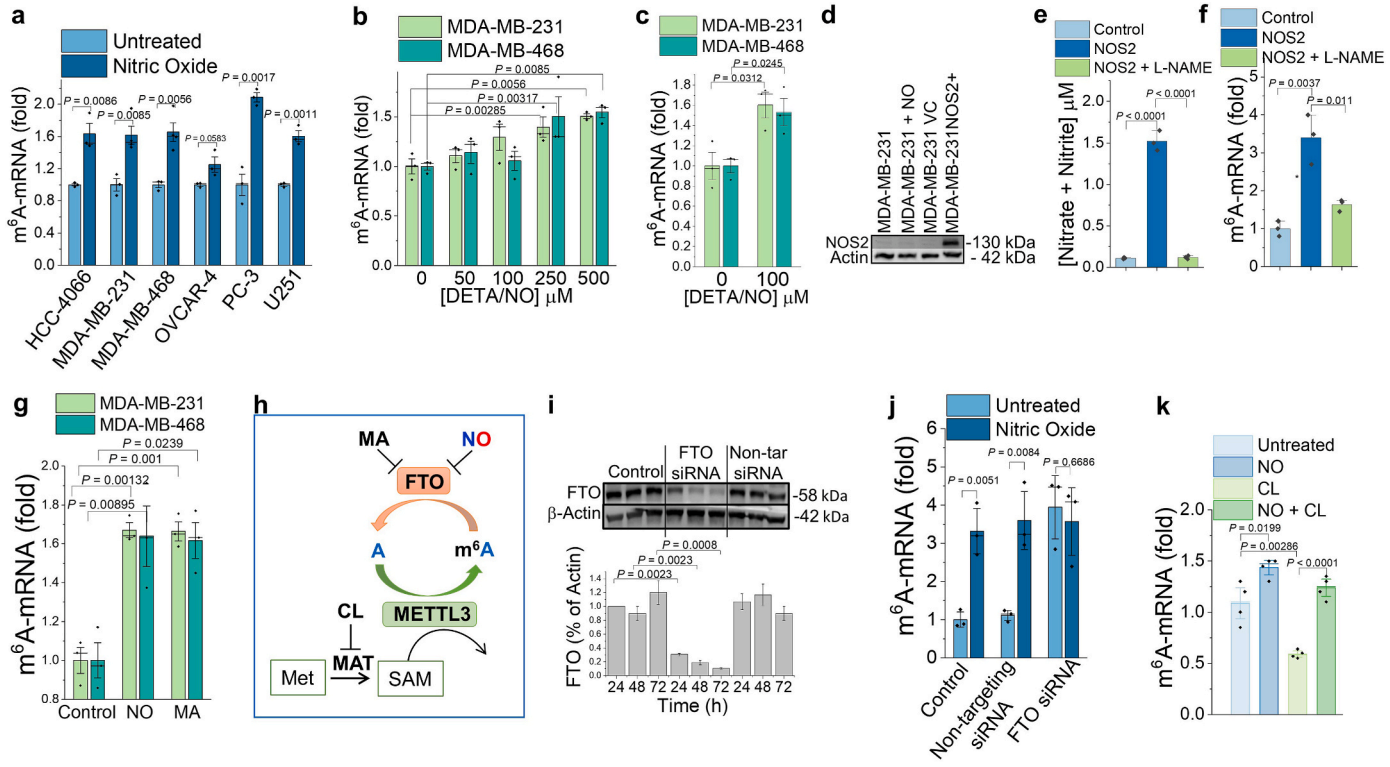


**Fig. 2. NO inhibits FTO and increases m$^6$A-mRNA in cancer cells. a**, Relative abundance of m$^6$A-mRNA in HCC4006 (lung), MDA-MB-231, -468 (TNBC), OVCAR-4 (ovarian), PC-3 (prostate), and U251 (glioblastoma) cancer cell lines that were treated without (light bars) or with (dark bars) NO (DETA/NO 500 μM, 24 h), ELISA. **b**, Total m$^6$A-mRNA in 2 TNBC cell lines (MDA-MB-231,-468) after 24 h dose course treatment with NO (DETA/NO), ELISA. **c**, Total m$^6$A-mRNA measured after 10 days of NO treatment (DETA/NO 100 μM), ELISA. **d**, Representative immunoblot for NOS2 protein in MDA-MB-231 ± DETA/NO (500 μM, 24 h), 231VC (transfected with empty vector control), and 231NOS2+ (transfected with NOS2 gene) cells. **e**, Accumulative NO synthesis (nitrite and nitrate) in the media of MDA-MB-231 (control) cells, 231NOS2+ (NOS2) cells, or 231NOS2+ cells treated with L-NAME (1 mM) after 24 h. **f**, Relative abundance of m$^6$A-mRNA in MDA-MB-231 (control) cells, 231NOS2+ (NOS2) cells, and 231NOS + cells treated with L-NAME (1 mM; 24 h), ELISA. **g**, Relative abundance of m$^6$A-mRNA in MDA-MB-231, and -468 cells after 24 h treatment with NO (500 μM DETA/NO) or the FTO inhibitor meclofenamic acid (MA, 100 μM), ELISA. DETA/NO and MA (IC50 8 μM) both achieve 100 % FTO inhibition at these concentrations. **h**, Schematic showing how inhibitors of METTL3 (methyltransferase) and FTO affect m$^6$A-mRNA levels. **i**, Representative immunoblot and densitometry for FTO in MDA-MB-231 cells (control), MDA-MD-231 cells transfected with FTO siRNA (FTO knockdown) or transfected with non-targeting siRNA (transfection control) and **j**, m$^6$A-mRNA levels in the same cells treated with or without NO (DETA/NO, 500 μM; 72 h), ELISA. **k**, m$^6$A-mRNA in MDA-MB-231 cells treated NO (DETA/NO 100 μM), or the METTL3 inhibitor cycloleucine (CL, 1 mM), or NO and CL together (n = 4), ELISA. **d,i**, cell lysates were prepared and immunoblotted with the indicated antibodies, data were independently replicated at least three times, with similar results. **a-c**, **e-g**, **j** n = 3 independent experiments. Data are represented as mean ± s.e.m., *P*-values were determined by unpaired two-tailed Student's *t*-tests, median line is shown.

treated with a non-targeting siRNA (Fig. 2J). NO treatment caused an increase in m$^6$A-mRNA in the control cells and cells treated with a non-targeting siRNA but did not further increase m$^6$A-mRNA in FTO-deficient cells. These findings suggest that NO mediates increases in m$^6$A-mRNA through inhibition of FTO activity.

Next, we asked whether NO was increasing m$^6$A-mRNA by increasing the activities of mRNA methyltransferases rather than by inhibiting demethylase activity. To test this, we treated cells with cycloleucine (CL), a competitive inhibitor of methionine adenosyltransferase which depletes the cell of S-adenosylmethionine, the substrate for RNA methyltransferases, such as METTL3 (Fig. 2H, K). Cells treated with CL alone had reduced levels of m$^6$A-mRNA; however, when NO was present during CL treatment, m$^6$A-mRNA levels remained elevated. These data suggest that NO is increasing m$^6$A-mRNA by a mechanism that cannot be attributed to increased mRNA methyltransferase activity. Lastly, we measured the expression levels of m$^6$A-mRNA methyltransferases (METTL3) and demethylases (FTO and ALKBH5) to determine if increases in m$^6$A-mRNA were due to NO-mediated changes in their relative levels of expression. Some genes exhibited transcriptional changes in response to NO, but there were no significant changes in protein expression for METTL3, FTO, or ALKBH5 (Supplemental Data Fig. 1).

### *2.3. Methylation of mRNA transcripts controls the expression of NO-regulated genes*

With the observation that NO directly inhibits FTO demethylase activity and globally increases m$^6$A-mRNA, we sought to decipher whether this was functionally associated with transcriptional changes in NO-regulated genes. First, we quantified changes in transcription by performing RNA-sequencing on samples from two cell lines treated chronically (10 days) with NO. In both cell lines, NO significantly up- and down-regulated several hundred genes (Fig. 3A). Gene Set Enrichment Analysis (GSEA) revealed that genes regulated by NO, and common to both cell types, were enriched in INFα response, TNFα signaling and other pathways (Fig. 3B). To identify which specific mRNA transcripts were enriched with m$^6$A, we conducted methylated RNA immunoprecipitation sequencing (MeRIP-seq) on mRNA extracted from MDA-MB-231 cells treated with NO for 10 days. Heatmap visualization demonstrated differential hypermethylated m$^6$A-mRNAs in the NO-treated vs. untreated cells (Fig. 3C). We also identified unique m$^6$A-methylated mRNA transcripts that were present only in the untreated sample (UT-only), only in the NO treated sample (NO-only), or in both NO and UT samples (Both NO and UT) (Fig. 3D).

Next, we determined if there were differences in the locations and amounts of m$^6$A on specific mRNA transcripts in each group. We found

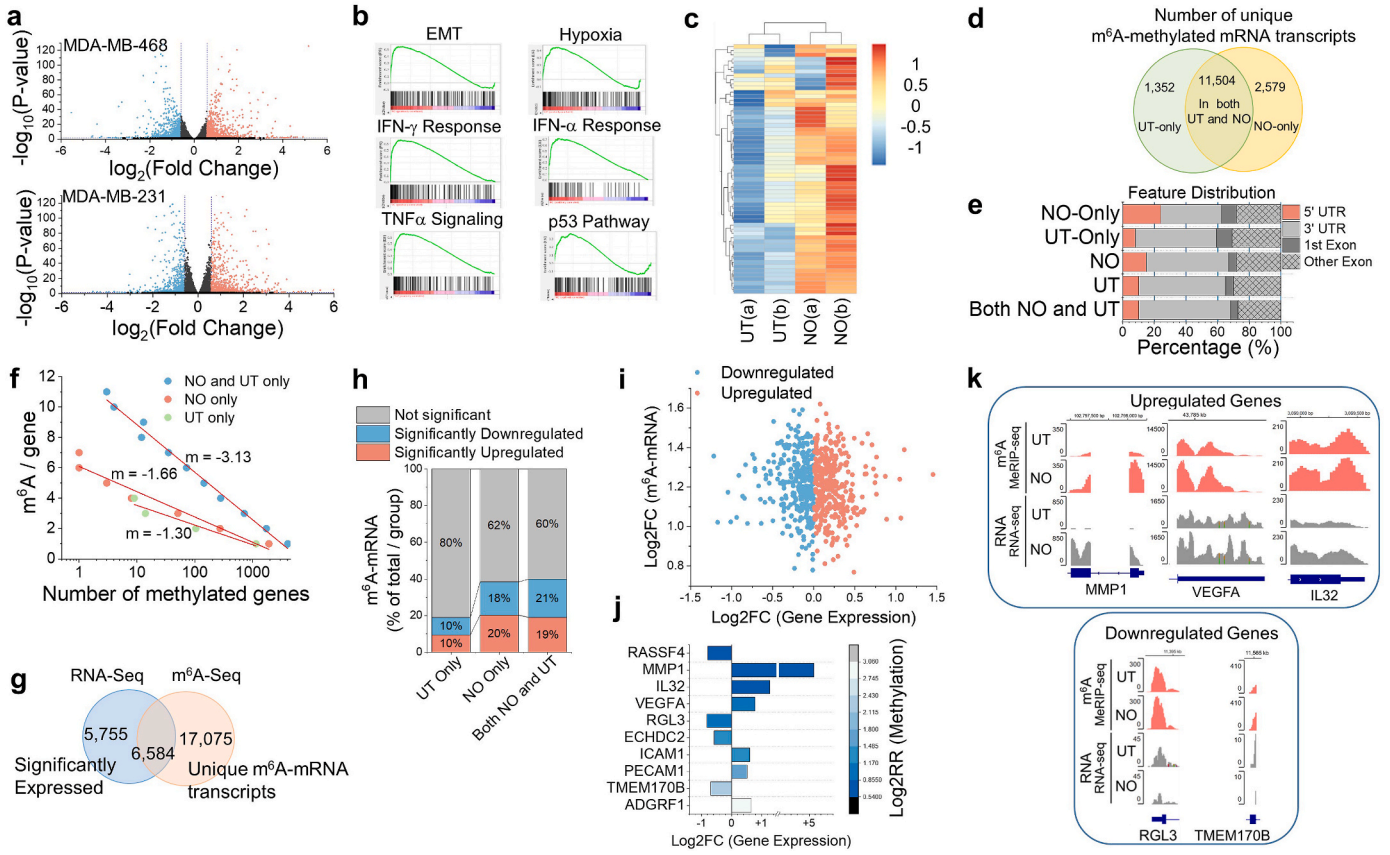


**Fig. 3. NO increases m$^6$A on mRNA of specific NO-regulated transcripts**. Cells were cultured with NO (DETA/NO 100 μM; 10 days). **a**, Volcano plots of NO-mediated mRNA changes in MDA-MB-468 (top) and MDA-MB-231 (bottom) cells. Significantly up- and down-regulated genes are indicated by red and blue respectively, n = 3 biologically independent samples for each cell type (*P*-values, and fold change as indicated). **b**, GSEA enrichment plots of top gene sets enriched in MDA-MB-231 and MDA-MB-468 cell lines. **c**, Heatmap of m$^6$A-mRNA from MeRIP-seq analysis of untreated (UT) and NO-treated (NO) MDA-MB-231 cells, (a) and (b) denote biological replicates, n = 2 (plot is the log2 FPKM value). **d**, Venn diagram of the number of unique m$^6$A-mRNAs that are in the untreated cells only (UT-only), the NO-treated cells only (NO-only), or that are common to both untreated and NO-treated cells (UT and NO). **e**, The locations (5′ UTR, 3′ UTR, 1st exon, or all other exons) of m$^6$A enrichment on mRNA as a percentage of all locations for each group. **f**, The relationship between the number of m$^6$A-methylated genes (mRNA transcripts) and the number of m$^6$A/gene for each group (UT-only, NO-only, and both UT and NO). **g**, Venn diagram demonstrating the overlap between the number of significantly expressed genes and the number of significantly m$^6$A-methylated genes for NO-treated vs. untreated cells. Significantly hypermethylated (log2.RR > 0 & adjusted p-value< 0.05) and significantly differentially expressed (Fold change adjusted p-value <0.05). **h**, The percentage of m$^6$A-methylated genes in each group that are associated with significant changes (up or down) in gene expression. **i**, Volcano plot of m$^6$A-mRNA methylation vs. gene expression change for the NO-only group. **j**, Magnitude and direction of gene expression for the tumor-associated mRNA transcripts that gain m$^6$A ($p < 0.05$), NO-only group. **k**, Representative Integrative Genomics Viewer (IGV) analysis of five of the NO-regulated mRNA transcripts demonstrating m$^6$A enrichment and up- or down-regulation of gene expression in MDA-MB-231 cells.

that transcripts in the "NO-only" group were significantly more enriched with m$^6$A in the 5′ UTR region (Fig. 3E) and also had a higher average number of methylated adenosine bases per mRNA transcript (1.66 for "NO-only" compared to 1.30 for "UT-only", Fig. 3F) compared to the "UT-only" group. To determine if m$^6$A was enriched in the mRNA transcripts of NO-responsive genes from cancer cells, we analyzed the m$^6$A-mRNA transcripts that were both hyper-methylated and demonstrated significant changes in gene expression (Fig. 3G). Almost twice as many methylated mRNA transcripts were associated with significant changes in gene expression in the "NO-only" (38 %) group compared to the "UT-only" group (20 %) (Fig. 3H). Of the total m$^6$A-mRNA transcripts in the "NO-only" group, 916 represented unique up- or down-regulated genes (Fig. 3I). Focusing on hyper-m$^6$A-methylated genes in this group, we saw that many of them were housekeeping yet a subset of upregulated genes were associated with tumor-promoting pathways while other downregulated genes were annotated to tumor-suppressing pathways (Fig. 3J and K).

To further evaluate whether NO-regulated m$^6$A-mRNA-associated transcriptional changes were downstream of FTO inhibition, we compared directional changes in gene expression in NO-treated and FTO-knockdown cells by RT-qPCR (Fig. 4A). We found that genes that were up- or down-regulated in the NO-treated cells were similarly up- or down-regulated in the FTO-knockdown cells. Next, we used a mouse xenograft NOS2-expressing tumor model to determine whether a defined set of NO-regulated m$^6$A-mRNA transcripts would show statistically significant differences in their expression levels between NO-producing and non–NO–producing tumors. Mice bearing NOS2-expressing MDA-MB-231 xenograft tumors were divided into two groups; half were treated with a aminoguanidine (AG), a selective inhibitor of NOS2, and the other half with saline (control). After 37 days of treatment, we measured tumoral levels of m$^6$A-mRNA and the expression of specific m$^6$A-regulated genes. In the NO-producing tumors, global m$^6$A-mRNA levels were increased compared to the tumors where NO synthesis was inhibited (Fig. 4B). Changes in gene expression in the NO-producing tumors were similar in magnitude and direction to the changes that were measured in the NO treated cells in culture (Fig. 4C).

## 3. Discussion

In this work, we revealed that physiologic NO concentrations

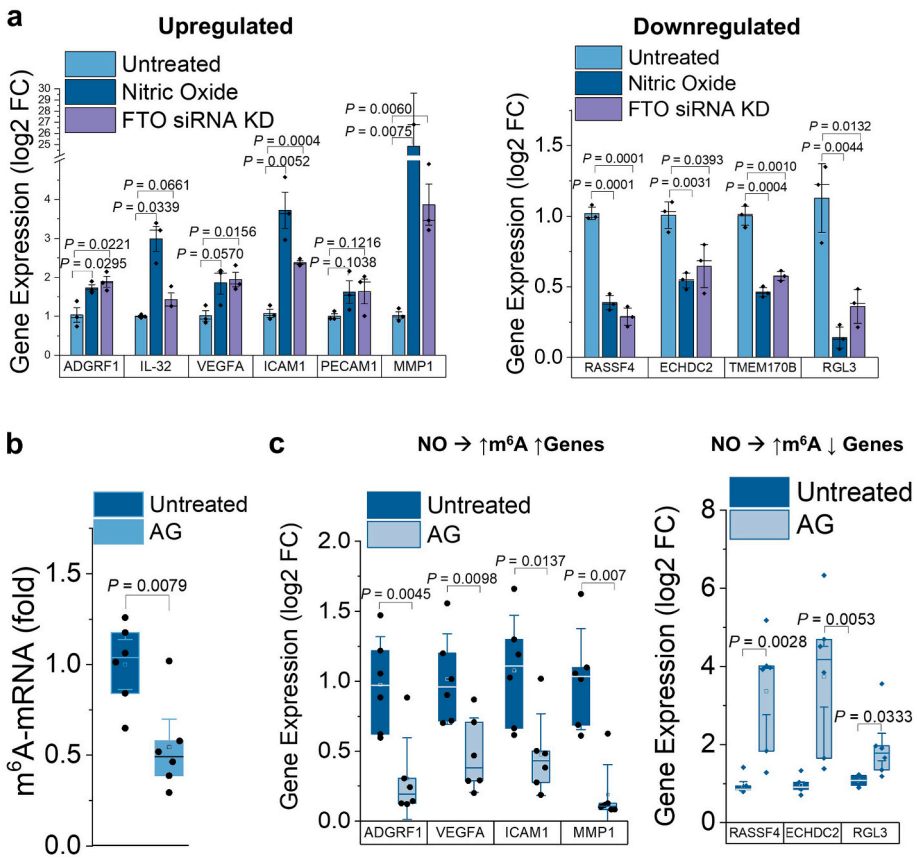


**Fig. 4. NO and FTO regulate the same m$^6$A-mRNA *in vitro* and *in vivo*.** **a**, mRNA expression (RT-qPCR) of select m$^6$A-methylated transcripts in untreated MDA-MB-231 cells (light blue bars), NO-treated MDA-MB-231 cells (DETA/NO; 500 μM, dark blue bars), and MDA-MB-231 FTO knockdown cells (purple bars) at 72 h. Methylated genes that are upregulated by NO are in the left panel and those that are downregulated by NO are in the right panel, n = 3 separate experiments. **b**, Relative m$^6$A-mRNA levels in MDA-MB-231 xenograft tumors from mice that had "NO-producing" tumors (untreated; dark blue bars), and from mice with tumors that did not synthesize NO, (treated with a NOS2 inhibitor aminoguanidine (AG) for 37 days, light bars), ELISA. **c,** mRNA expression (RT-qPCR) of genes from the same MDA-MB-231 xenograft tumors ( ± AG) for select genes that were m$^6$A-methylated and NO-regulated. Methylated genes that are upregulated by NO are in the left panel and methylated genes that are downregulated by NO are in the right panel. Data are represented as mean ± s.e.m., *P*-values were determined by unpaired two-tailed Student's *t*-tests, median line is shown, n = 6 mice/treatment group.

directly inhibit FTO via a novel mechanism involving DNIC assembly at the catalytic non-heme iron atom. We also demonstrated that in cancer cells exposed to exogeneous NO, or in cells endogenously synthesizing NO, global m$^6$A-mRNA levels are increased, and m$^6$A is enriched on specific NO-regulated mRNA transcripts.

The classical signaling mechanisms of NO, which are thought to underlie a majority of NO-mediated physiological signaling functions, are mediated through activation of sGC or by the formation of protein adducts containing nitrogen oxide functional groups (i.e., RSNO, nitrotyrosine). By demonstrating that NO inhibits FTO to drive m$^6$A-hypermethylation of transcriptionally regulated mRNA, we provide strong biochemical and transcriptomic evidence that NO is a bona fide endogenous regulator of the epitranscriptome. We lay out several lines of supportive evidence that suggest direct inhibition of FTO by NO is mechanistically responsible for increased m$^6$A-mRNA. We demonstrate that NO does not change the expression levels of m$^6$A-mRNA-modifying enzymes (methyltransferases and demethylases) and that inhibiting m$^6$A methyltransferases does not appreciably affect the ability of NO to increase relative levels of m$^6$A-mRNA. Moreover, inhibition or knockdown of FTO protein increased cellular m$^6$A-mRNA to similar levels as cells treated with NO alone, and m$^6$A-mRNA did not additively increase or significantly increase at all when FTO knockdown or FTO-inhibited cells were concurrently treated with NO. Genes transcriptionally up- or down-regulated by NO were also regulated in the same direction in cells where FTO was inhibited.

There are no structures of NO-bound to FTO and very little data on NO binding to any member of the large family of Fe(II)/2-OG-dependent proteins with the exception of two examples of the crystalline form demonstrating formation of the mono-NO at the iron site [57,58]. This is consistent with our initial hypothesis that NO would compete with, and replace, $O_2$ at the mononuclear iron center. However, since we demonstrate that FTO in solution binds two NO molecules we suspect that NO interferes with, or displaces, 2OG binding, providing a coordination site for a second NO molecule to bind and form the DNIC. In our cell culture experiments, the cells were grown at 21 % (~220 μM) $O_2$, and since we measured cellular inhibition of FTO when they were exposed to much lower steady-state concentrations of NO (nM), this suggests that FTO has a higher affinity for NO than for $O_2$. This could have important implications under conditions of reduced $O_2$, such as in a hypoxic tumor, where the minimum inhibitory concentration of NO for FTO would be expected to be even lower, further highlighting the physiological relevance of these results.

In general, gene transcription is a highly stochastic and dynamic process, and in heterogeneous tumors the mRNA copy number of any given gene can vary both between cells and across time. The experiments herein are the first to utilize cellular models of low physiologic steady-state concentrations of NO over an extended period of time (chronic 10-day treatment). This system more accurately replicates cellular responses to NO as would be seen in NOS2-positive tumors as well as epigenetic effects in general, which are mitotically heritable and should persist for multiple cell generations. Under conditions of chronic NO exposure, we demonstrated increased m$^6$A enrichment on specific

tumor-associated mRNA transcripts that were transcriptionally regulated by NO, suggesting that this may mechanistically play a role in establishing NO-mediated tumor phenotype. For example, a subset of genes that were hypermethylated and upregulated by NO are known drivers of cancer, including breast, when over-expressed (MMP1, IL32, ICAM1, PECAM1, ADGRF1, VEGFA [59–64]); genes that were hypermethylated and downregulated by NO are more typically associated with tumor suppressive functions and worse patient outcome when their tumoral expression levels are low (RASSF4, RGL3, ECHDC2, TMEM170B) [65–67].

A major question is whether this mechanism is specific and are these tumor-associated mRNAs recognized as functional targets of FTO in cancers. Results from this study cannot conclusively prove whether FTO inhibition by NO is a targeted mechanism to transcriptionally regulate specific genes, or if it represents a more generalized pathologic mechanism that drives tumor-permissive gene expression programs. In this regard, two points suggest some degree of specificity. The first is that enrichment of $m^6A$ is approximately 3 times greater at the 5′ UTR of mRNA in the NO-only group compared to the UT-only group. The second is that a greater proportion of mRNA transcripts in the NO-only group have multiple $m^6As$ per mRNA transcript. Studies have shown that both the number and distribution of $m^6A$ sites in mRNAs can regulate the transcriptome. Polymethylated $m^6A$-mRNAs provide a multivalent scaffold for the binding of YTH-domain $m^6A$ "reader" proteins, which are major determinants of mRNA translation and stability [68]. Notably, mRNAs that contain multiple annotated $m^6A$ sites are linked to distinctly different cellular functions and biological processes than singly methylated mRNAs [68]. Of the $m^6A$-mRNA NO-regulated genes, approximately equal amounts were up- and downregulated. Although this may simply reflect differences in transcriptional rates for specific genes, another possibility is that the abundance of specific mRNAs is being determined posttranscriptionally by the location, or degree, of $m^6A$ methylation, which can differentially affect mRNA metabolism.

How NO achieves this level of specificity and what it means in terms of the complex life cycle of individual mRNA transcripts may be partially determined by the cellular location of FTO. FTO is generally thought to be localized in the nucleus, yet its cellular distribution can vary widely, with up to 40 % of FTO demethylation occurring in the cytoplasm for some cell lines [69]. Although the kinetics are considerably slower, FTO can also demethylate $N^6$,2′-*O*-dimethyladenosine ($m^6A_m$) on mRNA and on snRNA, as well as $N^1$-methyladenosine ($m^1A$) on tRNA [69]. Because NO is uncharged and highly diffusible, it is generally assumed that it will be uniformly distributed within a cell. Therefore, the specificity of NO to affect the methylation status of specific mRNA transcripts may largely be a function of the distribution (nucleus vs. cytoplasm) of FTO and its specific mRNA substrates rather than an inherent NO-directed "specificity" of FTO for specific mRNAs.

It's important to note that there were 1352 $m^6A$-methylated mRNA transcripts representing 135 unique genes that were present only in the untreated control cells (UT-only). This suggests that these transcripts were either not present in the "NO-only" groups (i.e., downregulated) or that they were present but not methylated. Interestingly, 98 % of the "UT-only" $m^6A$-mRNA transcripts were still present (by RNA-seq) in the "NO-only" group, but not methylated. One possible explanation is that these transcripts represent nascent mRNAs that are more rapidly metabolized in the presence of NO but kinetically methylated more slowly. Some support for this theory comes from the fact that the $m^6A$-methylated transcripts in the UT-only group have fewer polymethylated sites and are only half as likely to be associated with significant transcriptional changes when compared to the NO-only group (20 % UT-Only vs. 38 % NO-only). However, due to the limitations of this study we cannot directly distinguish whether the UT-only transcripts have instead been demethylated in the NO-only group by an FTO-independent mechanism. For example, $m^6A$-mRNA can also be demethylated by ALKBH5, which is expressed in the cells we tested (Supplemental Data Fig. 1). It's possible that some mRNA transcripts are specifically demethylated by ALKBH5 but that cellular ALKBH5 is less sensitive to inhibition by NO. This is supported by the fact that only knocking down FTO closely replicates the effects of NO on global $m^6A$-mRNA levels, and on the regulation of specific $m^6A$-mRNA-associated genes.

In conclusion, this work provides foundational evidence that NO is an endogenous regulator of the epitranscriptome mediated by FTO-dependent changes in $m^6A$-mRNA. Other well-defined mechanisms of NO signaling require complex chemistry, such as those mediated by the formation *S*-nitrosothiols, yet the mechanism described herein is simple and direct. It requires NO synthesis, NO diffusion to FTO, and NO binding to the catalytic iron atom. We used cancer cells in this study to investigate the functional consequences of this non-canonical signaling mechanism, however, we anticipate that this epigenetic mechanism will have a causal impact on gene expression and cell phenotype in a variety of diseases. As NO and dysregulated $m^6A$-mRNA are independently associated with numerous pathologies (i.e., cancer, cardiovascular, inflammation, diabetes), results from this study suggest that the two variables are linked. Lastly, we hypothesize that these findings may have broader biological implications and may extend to include physiological gene regulation of a variety of normal cell types that can produce, or are exposed to, NO, such as smooth muscle, endothelial, hepatic, and neurons.

## 4. List of abbreviations

adenosine (A), AlkB Homolog 5 (ALKBH5), complementary DNA (cDNA), cyclic guanosine 3′,5′-monophosphate (cGMP), cycloleucine (CL), diethylamine nonoate (DEA/NO), diethylenetriamine NO donor (DETA/NO), dinitrosyl iron complex (DNIC), dithiothreitol (DTT), enzyme-linked immunosorbent assay (ELISA), electron paramagnetic resonance (EPR), ferrous iron (Fe(II)), fat mass- and obesity-associated protein (FTO), glyceraldehyde-3-phosphate dehydrogenase (GAPDH), 4-(2-hydroxyethyl)-1-piperazineethanesulfonic acid (HEPES), N (gamma)-nitro-L-arginine methyl ester (L-NAME), $N^6$-methyladenosine ($m^6A$), $N^6$, 2′-O-dimethyladenosine ($m^6A_m$), meclofenamic acid (MA), methylated RNA immunoprecipitation sequencing (meRIP-seq), methyltransferase (METTL), matrix metalloproteinase (MMP), messenger RNA (mRNA), nitric oxide (NO), nitrite ($NO_2^-$), nitrate ($NO_3^-$), nitric oxide synthase (NOS), ribonucleic acid (RNA), RNA-sequencing (RNA-seq), reverse transcription quantitative polymerase chain reaction (RT-qPCR), small interfering RNAs (siRNA), spermine NO donor (SPER/NO), triple negative breast cancer (TNBC), vascular endothelial growth factor (VEGF), YT521-B homology (YTH).

## 5. Methods

### 5.1. Chemicals

(Z)-1-[N-(2-aminoethyl)-N-(2-ammonioethyl)amino]diazen-1-ium-1,2-diolate (DETA/NO), (Z)-1-[N-[3-aminopropyl]-N-[4-(3-aminopropylammonio)butyl]-amino]diazen-1-ium-1,2-diolate (SPER/NO) (Gift from Dr. Joseph E. Saavedra (NCI)). N-(1-naphthyl)ethylenediamine dihydrochloride (NEDD) (Riedel-de Haen, Germany) and prepared to 0.1 % (w/v) in $H_2O$ and filtered to remove trace particles. Sulfanilamide (SULF; prepared to 2 % (w/v) in 5 % HCl and filtered to remove trace particles), ammonium iron(II) sulfate hexahydrate ($(NH_4)_2Fe(SO_4)2 \times 6H_2O$; purity 99.997 %), α-ketoglutaric acid sodium salt (αKG (2-OG); purity >98 %), (+)-sodium L-ascorbate (ascorbic acid; purity >98 %) (Sigma-Aldrich). Dithiothreitol (DTT) was purchased from Biorad. HEPES buffer (pH 7.2–7.5) (Gibco). Cycloleucine (purity >98 %) (Chem Impex). Meclofenamate sodium (MA) (Spectrum Chemical Manufacturing Corporation). N(G)-nitro-L-arginine methyl ester hydrochloride (L-NAME, purity >99 %) (Cayman Chemical).

### 5.2. Cell culture and treatment

Human triple negative breast cancer cell lines MDA-MB-231 and MDA-MB-468 and human glioblastoma cell line U251 were cultured in Dulbecco's modified Eagle's medium (DMEM; Gibco) supplemented with 10 % qualified fetal bovine serum (FBS; Gibco) and 1 % penicillin/streptomycin (P/S; Gibco). Human ovarian cancer cell line OVCAR4, prostate cancer cell line PC3, non-small cell lung cancer cell line HCC4006 were cultured in RPMI 1640 (Corning) supplemented with 10 % qualified fetal bovine serum (FBS; Gibco) and 1 % penicillin/streptomycin (P/S; Gibco). All cells were cultured at 37 °C in 5 % $CO_2$. Prior to use, cell line authentication was performed by short tandem repeat (STR) profiling and mycoplasma was tested at the University of Illinois at Chicago Genome Research Core. For experiments studying short response to NO (0–72 h), cells were grown to 80 % confluency and DETA/NO was added to the media to achieve physiologically relevant steady state NO concentrations (10–500 nM). For experiments studying chronic exposure to NO (10 days), cells were first plated with a density of $1.5 \times 10^6$ cells into 100 mm dishes. After 4 h of cell adherence, 100 μM of DETA/NO was added to the media and grown for 48 h. At this time, cells were collected with trypsin (Gibco), pooled according to each replicate, counted, and re-plated at the same starting density of $1.5 \times 10^6$ cells into new 100 mm dishes. This was repeated every 48 h for a total of 10 days of DETA/NO treatment.

MDA-MB-231 NOS2 expressing cells were a generous gift from Dr. Sharon Glynn (University of Galway). MDA-MB-231 cells were stably transduced with NOS2 lentiviral vector from Origene (MDA-MB-231-NOS2) or an empty vector (MDA-MB-231-VC) and cultured in RPMI 1640 (Corning) supplemented with 10 % qualified fetal bovine serum (FBS; Gibco) and 1 % penicillin/streptomycin (P/S; Gibco) at 37 °C in 5 % $CO_2$.

### 5.3. Griess assay to detect products of NO synthesis

To determine the amount of total NO produced by cells, we measured stable NO-oxidation products nitrate ($NO_3^-$) and nitrite ($NO_2^-$) by the Griess assay as previously described [70]. At experimental end points 100 μL of cell culture media was collected, transferred into a 96-well microplate, reagents were added, and absorbance was determined at 540 nm. The concentrations of nitrite were derived from regression analysis using serial dilutions of nitrate and nitrite standards.

### 5.4. $m^6A$ demethylation activity assay

$m^6A$ demethylase assay was performed with Epigenase $m^6A$ Demethylase Activity/Inhibition Assay Kit (EpiGentek) according to the manufacturer's instructions. Recombinant FTO protein was purchased from Active Motif (Cat. #31972). Briefly, the $m^6A$ demethylation reaction was performed in standard 50 μL of reaction mixture containing RNA with $m^6A$, 500 ng recombinant FTO, in demethylase buffer with necessary cofactors (Fe(II), 2OG, ascorbic acid). Inhibition reactions were performed with indicated concentrations of SPER/NO. The reaction was incubated at room temperature for 2 h. Remaining methylated ($m^6A$) substrate was recognized with a high affinity $m^6A$ antibody and incubated with detection antibody, and the signal was measured at 450 nm with an optional reference wavelength of 655 nm. The $m^6A$ signal intensity is inversely proportional to $m^6A$ demethylation activity.

### 5.5. Succinate demethylase assay

Demethylase activity was measured using the Succinate-Glo assay (Promega) following the manufacturer's procedure. Demethylation and hydroxylation reactions were carried out in 96-well white plates in 25 μL volumes using the demethylase/hydroxylase buffer, plus 10 μM substrate and 1 × acetoacetyl-CoA (supplied as 100 × in the kit). Recombinant FTO protein was purchased from BPS Biosciences (Cat. #79306), and ALKBH5 enzyme was purchased from Active Motif (Cat. #31589). Reactions were started by the addition of 12.5 μL of substrate mix containing 20 μM 2-OG, 2 × concentration of $m^6A$-RNA oligo (Dharmacon; Lafayette,CO), and 2 × acetoacetyl-CoA diluted in the demethylase/hydroxylase buffer. DETA/NO was serial diluted from 4 to 4000 μM, and the reaction ran for 90 min at 37 °C.

### 5.6. Electron paramagnetic resonance (EPR)

Recombinant FTO protein was from Active Motif (Cat. #31972), and a custom synthesized RNA oligo with internal $m^6A$ (sequence CUGGm [6]ACUGG) was purchased from Dharmacon (Lafayette,CO). The 60 μL reaction mixture containing $m^6A$ oligo (100 μM), FTO (50 μM), (NH4)2Fe(SO4)2 × 6H2O (500 μM), 2-OG (1 mM), ascorbic acid (1 mM), and DTT (1 mM) in 50 mM HEPES buffer (pH 7.2) was transferred to an X-band EPR tube with or without DEA/NO (25 μM). A small amount of sodium dithionite was added, and the reaction was incubated for 15 min at 37 °C, then flash frozen in liquid $N_2$. X-band continuous wave EPR spectroscopy using a Bruker ESP 300 spectrometer equipped with an Oxford Instruments ESR 910 continuous helium flow cryostat. Experimental parameters when searching for Fe(II)–NO signals were 10 K or 40 K, 9.37 GHz, 5 G modulation amplitude; for DNIC spectra were 77 K, 9.135 GHz, 10 G modulation amplitude.

### 5.7. Western blotting

Treated cells were washed with cold 1X phosphate-buffered saline (PBS; Sigma), and whole cell lysates were extracted using RIPA lysis buffer system (Santa Cruz) containing lysis buffer, PMSF, protease inhibitor cocktail, and sodium orthovanadate. Lysates were centrifuged for 10 min at 4 °C at 10,000 g. Protein concentrations were estimated using DC Protein Assay Reagents (Biorad) according to manufacturer's instructions. Cell lysates (20–40 μg) were resolved by SDS-PAGE (Biorad) and transferred onto PVDF membranes using the iBlot™ transfer system (Invitrogen). Membranes were blocked for 1 h with 5 % milk in PBS containing 0.1 % Tween 20 and incubated overnight at 4 °C with suitable primary antibodies (Supplemental Data Table I). Membranes were washed with PBS containing 0.1 % Tween 20, incubated for 1 h with appropriate secondary antibodies. Blots were imaged in a FluorChem E system (ProteinSimple) and developed using SuperSignal chemiluminescent substrates (Thermo Fisher Scientific).

### 5.8. RNA extraction and quantitative RT-qPCR analysis

Total RNA were isolated using the RNAqueous™-4PCR kit (Ambion). All samples were treated with DNase I to avoid genomic DNA contaminations, 1 μg of RNA was reverse-transcribed using iScript™ cDNA Synthesis kit (Biorad) following standard manufacturer's protocols. PCR was performed using Fast SYBR™ Green Master Mix (Applied Biosystems) on the CFX Connect Real-Time PCR Detection System (Biorad). GAPDH or β-actin was used as the housekeeping control, and all samples were run in triplicate. Data was processed using the $2-\Delta\Delta Ct$ method. Oligonucleotide primer sequences can be found in (Supplemental Data Table II).

### 5.9. $m^6A$-mRNA quantification

mRNA was extracted from cells using NEB Magnetic mRNA Isolation kit (New England Biolabs) and treated with DNase I (Ambion) to avoid genomic DNA contaminations. 200 ng of mRNA was measured using EpiQuik $m^6A$ RNA Methylation Quantification Kit (Epigentek). All samples were tested in technical duplicate. Sample Absorbance was measured at 450 nm and the $m^6A$ levels were calculated relative to a positive control according to manufacturer's instructions.

### 5.10. siRNA transfection

MDA-MB-231 cells were plated at 0.25 × $10^6$ cells/well into 6-well plates in a total volume of 2 mL media and 60–80 % confluence at transfection. Cells were then transfected with either 37.5 nM scrambled control or FTO siRNA (Silencer Select; Invitrogen) using Lipofectamine 3000 transfection reagent (Invitrogen) according to the manufacturer's instructions. After growing overnight, transfected cells were treated with 0 or 500 μM DETA/NO for 24–72 h. To measure FTO knockdown efficiency, protein was extracted and FTO was quantified by immunoblotting.

### 5.11. RNA preparation and RNA-sequencing

Total RNAs were isolated using the RNAqueous™-4PCR kit (Ambion) and treated with DNase I (Ambion) to avoid genomic DNA contaminations. Libraries were prepared with KAPA RNA Hyper Prep kit (Roche). The libraries were pooled, quantitated by qPCR, and then sequenced on the NovaSeq 6000 (Illumina) to generate 100-bp single reads. The sequencing depth for each sample was >30 million reads. Library preparations and sequencing was performed by the Roy J. Carver Biotechnology Center (CBC; Champaign, IL).

### 5.12. $m^6A$-mRNA immunoprecipitation and $m^6A$-RIP-sequencing

The $m^6A$ immunoprecipitation procedure was modified from previously reported methods [71]. mRNA was isolated following three rounds of NEB Magnetic mRNA Isolation (New England Biolabs) and treated with DNase I (Ambion) to avoid genomic DNA contaminations. A small amount of each mRNA sample was run on a 1.5 % agarose gel to confirm purity and absence of rRNA. mRNA was subsequently fragmented into 150–300 nt fragments by incubating samples at 94 °C for 90s in fragmentation buffer (100 mM Tris-HCl pH 7.0, 100 mM $ZnCl_2$) then stopped by addition of 0.5 M EDTA. RNA fragments were concentrated by RNA Clean & Concentrator kit (Zymo Research). About 1 μg of fragmented RNA was saved for input control. For immunoprecipitation, 50 μL Protein G Dynabeads (Invitrogen) were prepared according to manufacturer's protocol and resuspended in 1X immunoprecipitation buffer (50 mM Tris-HCl pH 7.4, 750 mM NaCl, 0.5 % Igepal CA-630 in RNase-free $H_2O$) then incubated with 10 μg of anti-$m^6A$ antibody (1 μg/μL in PBS; Synaptic Systems) for 30 min at 4 °C. Fragmented RNA was prepared in immunoprecipitation buffer (1X IP; 50 mM Tris-HCl pH 7.4, 750 mM NaCl, 0.5 % Igepal CA-630 in RNase-free $H_2O$) and denatured for 2 min at 70 °C then kept on ice. Following two washes with 1X IP buffer, beads were resuspended with fragmented RNA solution and incubated at 4° for 2 h with end-over-end rotation. RNA-bound beads were then washed with two rounds of each: 1X IP buffer, Low Salt buffer (10 mM Tris-HCl pH 7.4, 10 mM NaCl, 0.1 % Igepal CA-630 in RNase-free $H_2O$), then High Salt buffer (10 mM Tris-HCl pH 7.4, 500 mM NaCl, 0.1 % Igepal CA-630 in RNase-free $H_2O$) before eluting with Buffer RLT (QIAGEN). Eluted $m^6A$-mRNA was concentrated by RNA Clean & Concentrator kit (Zymo Research). Libraries were prepared with KAPA RNA Hyper Prep kit (Roche). The libraries were pooled, quantitated by qPCR, and then sequenced on the NovaSeq 6000 (Illumina) to generate 150-bp paired-end reads. The sequencing depth for each sample was between 45 and 95 million reads. Library preparations and sequencing was performed by the Roy J. Carver Biotechnology Center (CBC; Champaign, IL).

### 5.13. Statistical analysis

Data in the graphs were presented as mean ± standard error of the mean which was obtained from a minimum of three independent experiments unless otherwise noted. Statistical analysis was performed using either student's t-test or one-way analysis of variance with Bonferoni post hoc analysis using OriginPro software.

### 5.14. Sequencing

Read Quality Assessment and Filtering. Basic assessment of Illumina output reads quality (FastQ) including GC bias were checked by FastQC (v0.11.9) program. Poor quality reads were eliminated before mapping based on default quality flag by Illumina pipeline in FastQ file. FastQC quality analysis results were summarized using MultiQC (v1.14) [72].

### 5.15. RNA-seq alignment and analysis

Mapping of reads. Single-end reads were mapped to human reference genome GRCh38 with TopHat (version 2.1.1)[73] and Bowtie (version 2.5.0.0) [74]. Identified average 150bp short reads were uniquely aligned allowing at best two mismatches, 0 splice-mismatches and no-duplicates (-N 2 -M -g 1) [75]. Sequences aligned to more than one location with equal quality were discarded to avoid bias. The reads that were not mapped to the genome were utilized to map against the transcriptome (junctions mapping). EnsEMBL version 109 [75] gene model was used for this process. Normalized BedGraph and BigWig count files, read density plots were generates using deepTools (version 3.5.1) [76]. *Read count, normalization and differential expression analysis.* After mapping, we used SubRead package featureCount (version 2.0.3; [77]) to calculate absolute read abundance for each transcript/gene associated with EnsEMBL (v109) genes of *Homo sapiens*. For differential expression (DE) analysis, we used Bioconductor [78] package DESeq2 (version 1.38.3) with R version 4.2.2 (2022-10-31); [79]) that utilizes a model based on the negative binomial distribution. To avoid false positives, we considered only those transcripts where at least 10 reads are annotated in at least one of the samples used in this study.

### 5.16. $m^6A$-RIP-seq data alignment and analysis

Mapping of reads. Paired-end reads were mapped to human GRCh38 genome reference genome using TopHat (version: 2.1.1)[73] and Bowtie (version 2.5.0.0)[74]. Identified average 150bp short reads were uniquely aligned allowing at best two mismatches, 0 splice-mismatches, with no-duplicates nor multimapping allowed (-N 2 -M -g 1)[75]. Sequences aligned to more than one location with equal quality were discarded to avoid bias. Reads not mapped to the genome were utilized to map against the transcriptome (junctions mapping) using EnsEMBL version 109 [75] gene model. *Genome coverage:* Read depth and coverage were assessed using RseQC (version 2.6.4) tool [80]. Mapping quality, duplicate removal, and indexing were performed using samtools (version 1.13) [81]. Normalized BedGraph and BigWig count files as well as read density plots were generates using deepTools (version 3.5.1) [76].

### 5.17. Peak calling, differential methylation & peak annotation

Peak calling from the aligned files was performed in R (version 4.2.2; 2022-10-31) using Bioconductor [78] package TRESS (v1.5.0) (Toolbox for mRNA Epigenetics Sequencing analysiS) [82], designed for analysis of MeRIP-seq data. It provides functionalities for identification of $m^6A$ and differential $m^6A$ methylation. Overlap of peaks were analyzed using bedtools (v 2.30.0)[83]. Peaks were annotated to genomic location/coordinates using ChIPseeker [84] and bedtools. PCA plots were created using the read counts in each called peak location in each sample (including input and ChIP) to assess replicate consistency (data not shown).

### 5.18. Gene set enrichment analysis (GSEA)

We used Gitools for enrichment analysis and heatmap generation [85]. Resulting p-values were adjusted for multiple testing using the Benjamin and Hochberg's method of False Discovery Rate (FDR) [86]. Gene set enrichment analysis (GSEA). Ranked Gene Set Enrichment

Analysis (GSEA) [87,88] was performed with software version 4.2.2 [build: 8] which uses predefined gene sets from the Molecular Signatures Database Human MSigDB v2023.1.Hs. We used collection sets C1–C7 for GSEA analysis and identify groups of genes that shared common pathways and functions in both MDA-MB-231 and MDA-MB-468 RNA-seq data sets. The minimum and maximum criteria for selection of gene sets from the collection were 10 and 500 genes, respectively.

### 5.19. Mouse xenograft

Female athymic nude mice were injected with 750,000 GFP-tagged MDA-MB-231 human breast cancer cells in the mammary fat pad at 9–10 weeks of age and grown for 1 week before administration of the NOS2 inhibitor AG. Half the mice (10 in each group) were administered ad libitum the NOS2 inhibitor aminoguanidine (AG) in filter-sterilized drinking water at 0.5 g/L. After 37 days tumor tissue was extracted and frozen at −80 °C until further study. To isolate mRNA, 10 mg of tumor tissue was disrupted by Mini-Beadbeater-16 (Biospec), and mRNA was isolated using NEB Magnetic mRNA Isolation kit (New England Biolabs), and $m^6A$ mRNA was quantified.

## Author contributions

D.T. conceived and supervised the project. H.K. and M.P. performed the *in vitro* and *in vivo* experiments (immunoblots, ELISA, etc.). H.K., B. H., and D.T. participated in experimental design and data analysis. B.H. performed the EPR analysis. S.G. provided the NOS2 cells and technical advice. M.M., X.W., A.I. and E.B. conducted the sequencing analysis. D. T. and H. K. wrote the manuscript with input from all coauthors.

## Declaration of competing interest

None.

## Data availability

Data will be made available on request.

## Acknowledgements

University of Illinois Chicago Department of Pharmaceutical Sciences Bridge Fund, Hans W. Vahlteich Bridge Fund, University of Illinois at Chicago Drug Discovery Center (UICentre), and the University of Illinois Cancer Center Data Integration Shared Resource (DISR).

## Appendix A. Supplementary data

Supplementary data to this article can be found online at https://doi.org/10.1016/j.redox.2023.102928.

## References

[1] J.R. Hickok, D. Vasudevan, K. Jablonski, D.D. Thomas, Oxygen dependence of nitric oxide-mediated signaling, Redox Biol. 1 (2013) 203–209.
[2] V. Somasundaram, et al., Molecular mechanisms of nitric oxide in cancer progression, signal transduction, and metabolism, Antioxidants Redox Signal. 30 (2019) 1124–1143.
[3] D.D. Thomas, Breathing new life into nitric oxide signaling: a brief overview of the interplay between oxygen and nitric oxide, Redox Biol. 5 (2015) 225–233.
[4] J.R. Hickok, D. Vasudevan, G.R. Thatcher, D.D. Thomas, Is S-nitrosocysteine a true surrogate for nitric oxide? Antioxidants Redox Signal. 17 (2012) 962–968.
[5] C.T. Stomberski, D.T. Hess, J.S. Stamler, Protein S-nitrosylation: determinants of specificity and enzymatic regulation of S-Nitrosothiol-Based signaling, Antioxidants Redox Signal. 30 (2019) 1331–1351.
[6] V.T. Dao, et al., Non-canonical chemical feedback self-limits nitric oxide-cyclic GMP signaling in health and disease, Sci. Rep. 10 (2020), 10012.
[7] A.M.S. Yamashita, et al., Balance between S-nitrosylation and denitrosylation modulates myoblast proliferation independently of soluble guanylyl cyclase activation, Am. J. Physiol. Cell Physiol. 313 (2017) C11–C26.
[8] D.D. Thomas, et al., Signaling and stress: the redox landscape in NOS2 biology, Free Radic. Biol. Med. 87 (2015) 204–225.
[9] C.L. McGinity, et al., Nitric oxide modulates metabolic processes in the tumor immune microenvironment, Int. J. Mol. Sci. 22 (2021).
[10] J.R. Hickok, D.D. Thomas, Nitric oxide and cancer therapy: the emperor has NO clothes, Curr. Pharmaceut. Des. 16 (2010) 381–391.
[11] D. Vasudevan, D.D. Thomas, Insights into the diverse effects of nitric oxide on tumor biology, Vitam. Horm. 96 (2014) 265–298.
[12] S. Loibl, et al., The role of early expression of inducible nitric oxide synthase in human breast cancer, Eur. J. Cancer 41 (2005) 265–271.
[13] B. De Paepe, V.M. Verstraeten, C.R. De Potter, G.R. Bullock, Increased angiotensin II type-2 receptor density in hyperplasia, DCIS and invasive carcinoma of the breast is paralleled with increased iNOS expression, Histochem. Cell Biol. 117 (2002) 13–19.
[14] J.L. Heinecke, et al., Tumor microenvironment-based feed-forward regulation of NOS2 in breast cancer progression, Proc. Natl. Acad. Sci. U. S. A. 111 (2014) 6323–6328.
[15] C.H. Switzer, et al., Ets-1 is a transcriptional mediator of oncogenic nitric oxide signaling in estrogen receptor-negative breast cancer, Breast Cancer Res. 14 (2012) R125.
[16] L.A. Ridnour, et al., Nitric oxide synthase and breast cancer: role of TIMP-1 in NO-mediated Akt activation, PLoS One 7 (2012), e44081.
[17] C.H. Switzer, et al., S-nitrosation mediates multiple pathways that lead to tumor progression in estrogen receptor-negative breast cancer, For Immunopathol Dis Therap 3 (2012) 117–124.
[18] C.H. Switzer, et al., Nitric oxide and protein phosphatase 2A provide novel therapeutic opportunities in ER-negative breast cancer, Trends Pharmacol. Sci. 32 (2011) 644–651.
[19] S.A. Glynn, et al., Increased NOS2 predicts poor survival in estrogen receptor-negative breast cancer patients, J. Clin. Invest. 120 (2010) 3843–3854.
[20] R.L. Prueitt, et al., Inflammation and IGF-I activate the Akt pathway in breast cancer, Int. J. Cancer 120 (2007) 796–805.
[21] R.Y.S. Cheng, et al., Interferon-gamma is quintessential for NOS2 and COX2 expression in ER(-) breast tumors that lead to poor outcome, Cell Death Dis. 14 (2023) 319.
[22] V. Somasundaram, et al., Systemic Nos2 Depletion and Cox inhibition limits TNBC disease progression and alters lymphoid cell spatial orientation and density, Redox Biol. 58 (2022), 102529.
[23] P.F. Liu, et al., The clinical value of exhaled nitric oxide in patients with lung cancer, Clin. Res. J 12 (2018) 23–30.
[24] L. Zhang, et al., Upregulation of cytoskeleton protein and extracellular matrix protein induced by stromal-derived nitric oxide promotes lung cancer invasion and metastasis, Curr. Mol. Med. 14 (2014) 762–771.
[25] X. Gao, et al., Nitric oxide metabolites and lung cancer incidence: a matched case-control study nested in the esther cohort, Oxid. Med. Cell. Longev. 2019 (2019), 6470950.
[26] K.M. Lee, et al., Nitric oxide synthase gene polymorphisms and prostate cancer risk, Carcinogenesis 30 (2009) 621–625.
[27] A. Erlandsson, et al., High inducible nitric oxide synthase in prostate tumor epithelium is associated with lethal prostate cancer, Scand J. Urol. 52 (2018) 129–133.
[28] A.J. Burke, et al., Chronic nitric oxide exposure induces prostate cell carcinogenesis, involving genetic instability and a pro-tumorigenic secretory phenotype, Nitric Oxide 127 (2022) 44–53.
[29] J.M. Fahey, W. Korytowski, A.W. Girotti, Upstream signaling events leading to elevated production of pro-survival nitric oxide in photodynamically-challenged glioblastoma cells, Free Radic. Biol. Med. 137 (2019) 37–45.
[30] M.A. Altinoz, I. Elmaci, Targeting nitric oxide and NMDA receptor-associated pathways in treatment of high grade glial tumors. Hypotheses for nitro-memantine and nitrones, Nitric Oxide 79 (2018) 68–83.
[31] M.A. Puglisi, et al., High nitric oxide production, secondary to inducible nitric oxide synthase expression, is essential for regulation of the tumour-initiating properties of colon cancer stem cells, J. Pathol. 236 (2015) 479–490.
[32] G.A. de Oliveira, et al., Inducible nitric oxide synthase in the carcinogenesis of gastrointestinal cancers, Antioxidants Redox Signal. 26 (2017) 1059–1077.
[33] D. Drehmer, et al., Nitric oxide favours tumour-promoting inflammation through mitochondria-dependent and -independent actions on macrophages, Redox Biol. 54 (2022), 102350.
[34] D.A. Goncalves, et al., Imbalance between nitric oxide and superoxide anion induced by uncoupled nitric oxide synthase contributes to human melanoma development, Int. J. Biochem. Cell Biol. 115 (2019), 105592.
[35] D. Massi, et al., Inducible nitric oxide synthase expression in melanoma: implications in lymphangiogenesis, Mod. Pathol. 22 (2009) 21–30.
[36] E. Lopez-Rivera, et al., Inducible nitric oxide synthase drives mTOR pathway activation and proliferation of human melanoma by reversible nitrosylation of TSC2, Cancer Res. 74 (2014) 1067–1078.
[37] R. Eller-Borges, et al., Bradykinin promotes murine melanoma cell migration and invasion through endogenous production of superoxide and nitric oxide, Nitric Oxide 132 (2023) 15–26.
[38] R. Wang, et al., iNOS promotes CD24(+)CD133(+) liver cancer stem cell phenotype through a TACE/ADAM17-dependent Notch signaling pathway, Proc. Natl. Acad. Sci. U. S. A. 115 (2018), E10127-E10136.
[39] Y.H. Park, et al., iNOS promotes HBx-induced hepatocellular carcinoma via upregulation of JNK activation, Biochem. Biophys. Res. Commun. 435 (2013) 244–249.

[40] D. Wiener, S. Schwartz, The epitranscriptome beyond m(6)A, Nat. Rev. Genet. 22 (2021) 119–131.
[41] E. Sendinc, Y. Shi, RNA m6A methylation across the transcriptome, Mol. Cell 83 (2023) 428–441.
[42] S. Liu, et al., METTL3 plays multiple functions in biological processes, Am. J. Cancer Res. 10 (2020) 1631–1646.
[43] S. Relier, E. Rivals, A. David, The multifaceted functions of the Fat mass and Obesity-associated protein (FTO) in normal and cancer cells, RNA Biol. 19 (2022) 132–142.
[44] D. Schmidl, N.S.W. Jonasson, A. Menke, S. Schneider, L. Daumann, Spectroscopic and in vitro investigations of Fe2+/alpha-Ketoglutarate-dependent enzymes involved in nucleic acid repair and modification, Chembiochem (2022).
[45] W. Ma, T. Wu, RNA m6A modification in liver biology and its implication in hepatic diseases and carcinogenesis, Am. J. Physiol. Cell Physiol. 323 (2022) C1190–C1205.
[46] V. Sikorski, A. Vento, E. Kankuri, I.-E. Consortium, Emerging roles of the RNA modifications N6-methyladenosine and adenosine-to-inosine in cardiovascular diseases, Mol. Ther. Nucleic Acids 29 (2022) 426–461.
[47] H. Zhong, H.F. Tang, Y. Kai, N6-methyladenine RNA modification (m(6)A): an emerging regulator of metabolic diseases, Curr. Drug Targets 21 (2020) 1056–1067.
[48] Q. Lan, et al., The critical role of RNA m(6)A methylation in cancer, Cancer Res. 79 (2019) 1285–1292.
[49] Y. Wang, et al., Emerging roles of N6-methyladenosine (m(6)A) modification in breast cancer, Cell Biosci. 10 (2020) 136.
[50] C. Gu, et al., RNA m(6)A modification in cancers: molecular mechanisms and potential clinical applications, Innovation 1 (2020), 100066.
[51] S.C. Baksh, L.W.S. Finley, Metabolic coordination of cell fate by alpha-ketoglutarate-dependent dioxygenases, Trends Cell Biol. 31 (2021) 24–36.
[52] S. Martinez, R.P. Hausinger, Catalytic mechanisms of Fe(II)- and 2-Oxoglutarate-dependent oxygenases, J. Biol. Chem. 290 (2015) 20702–20711.
[53] J.C. Pereira, A.V. Iretskii, R.M. Han, P.C. Ford, Dinitrosyl iron complexes with cysteine. Kinetics studies of the formation and reactions of DNICs in aqueous solution, J. Am. Chem. Soc. 137 (2015) 328–336.
[54] J.R. Hickok, et al., Dinitrosyliron complexes are the most abundant nitric oxide-derived cellular adduct: biological parameters of assembly and disappearance, Free Radic. Biol. Med. 51 (2011) 1558–1566.
[55] T.P. Reddy, S.A. Glynn, T.R. Billiar, D.A. Wink, J.C. Chang, Targeting nitric oxide: say NO to metastasis, Clin. Cancer Res. 29 (2023) 1855–1868.
[56] Y. Huang, et al., Meclofenamic acid selectively inhibits FTO demethylation of m6A over ALKBH5, Nucleic Acids Res. 43 (2015) 373–384.
[57] Z. Zhang, et al., Crystal structure of a clavaminate synthase-Fe(II)-2-oxoglutarate-substrate-NO complex: evidence for metal centered rearrangements, FEBS Lett. 517 (2002) 7–12.
[58] P.L. Roach, et al., Structure of isopenicillin N synthase complexed with substrate and the mechanism of penicillin formation, Nature 387 (1997) 827–830.
[59] A. Player, et al., Identification of candidate genes associated with triple negative breast cancer, Genes Cancer 8 (2017) 659–672.
[60] C.J. Shen, Y.L. Kuo, C.C. Chen, M.J. Chen, Y.M. Cheng, MMP1 expression is activated by Slug and enhances multi-drug resistance (MDR) in breast cancer, PLoS One 12 (2017), e0174487.
[61] P. Guo, et al., A rationally designed ICAM1 antibody drug conjugate eradicates late-stage and refractory triple-negative breast tumors in vivo, Sci. Adv. 9 (2023), eabq7866.
[62] Z. Qiu, et al., Roles of intercellular cell adhesion molecule-1 (ICAM-1) in colorectal cancer: expression, functions, prognosis, tumorigenesis, polymorphisms and therapeutic implications, Front. Oncol. 12 (2022), 1052672.
[63] N.M. Abdulkareem, et al., A novel role of ADGRF1 (GPR110) in promoting cellular quiescence and chemoresistance in human epidermal growth factor receptor 2-positive breast cancer, Faseb. J. 35 (2021), e21719.
[64] X. Cao, J. Geradts, M.W. Dewhirst, H.W. Lo, Correction: upregulation of VEGF-A and CD24 gene expression by the tGLI1 transcription factor contributes to the aggressive behavior of breast cancer cells, Oncogene 41 (2022) 1225–1226.
[65] Y. Han, et al., RASSF4 inhibits cell proliferation and increases drug sensitivity in colorectal cancer through YAP/Bcl-2 pathway, J. Cell Mol. Med. 26 (2022) 3538–3547.
[66] G.R. Ehrhardt, C. Korherr, J.S. Wieler, M. Knaus, J.W. Schrader, A novel potential effector of M-Ras and p21 Ras negatively regulates p21 Ras-mediated gene induction and cell growth, Oncogene 20 (2001) 188–197.
[67] M. Li, et al., Transmembrane protein 170B is a novel breast tumorigenesis suppressor gene that inhibits the Wnt/beta-catenin pathway, Cell Death Dis. 9 (2018) 91.
[68] R.J. Ries, et al., m(6)A enhances the phase separation potential of mRNA, Nature 571 (2019) 424–428.
[69] J. Wei, et al., Differential m(6)A, m(6)A(m), and m(1)A demethylation mediated by FTO in the cell nucleus and cytoplasm, Mol. Cell 71 (2018) 973–985 e5.
[70] K.M. Miranda, M.G. Espey, D.A. Wink, A rapid, simple spectrophotometric method for simultaneous detection of nitrate and nitrite, Nitric Oxide 5 (2001) 62–71.
[71] D. Dominissini, S. Moshitch-Moshkovitz, M. Salmon-Divon, N. Amariglio, G. Rechavi, Transcriptome-wide mapping of N(6)-methyladenosine by m(6)A-seq based on immunocapturing and massively parallel sequencing, Nat. Protoc. 8 (2013) 176–189.
[72] P. Ewels, M. Magnusson, S. Lundin, M. Kaller, MultiQC: summarize analysis results for multiple tools and samples in a single report, Bioinformatics 32 (2016) 3047–3048.
[73] C. Trapnell, L. Pachter, S.L. Salzberg, TopHat: discovering splice junctions with RNA-Seq, Bioinformatics 25 (2009) 1105–1111.
[74] B. Langmead, S.L. Salzberg, Fast gapped-read alignment with Bowtie 2, Nat. Methods 9 (2012) 357–359.
[75] T.J. Hubbard, et al., Ensembl 2007, Nucleic Acids Res. 35 (2007) D610–D617.
[76] F. Ramirez, et al., deepTools2: a next generation web server for deep-sequencing data analysis, Nucleic Acids Res. 44 (2016) W160–W165.
[77] Y. Liao, G.K. Smyth, W. Shi, The Subread aligner: fast, accurate and scalable read mapping by seed-and-vote, Nucleic Acids Res. 41 (2013) e108.
[78] R.C. Gentleman, et al., Bioconductor: open software development for computational biology and bioinformatics, Genome Biol. 5 (2004) R80.
[79] S. Anders, W. Huber, Differential expression analysis for sequence count data, Genome Biol. 11 (2010) R106.
[80] L. Wang, S. Wang, W. Li, RSeQC: quality control of RNA-seq experiments, Bioinformatics 28 (2012) 2184–2185.
[81] P. Danecek, et al., Twelve years of SAMtools and BCFtools, GigaScience 10 (2021).
[82] Z. Guo, A.M. Shafik, P. Jin, Z. Wu, H. Wu, Analyzing mRNA epigenetic sequencing data with TRESS, Methods Mol. Biol. 2624 (2023) 163–183.
[83] A.R. Quinlan, I.M. Hall, BEDTools: a flexible suite of utilities for comparing genomic features, Bioinformatics 26 (2010) 841–842.
[84] G. Yu, L.G. Wang, Q.Y. He, ChIPseeker: an R/Bioconductor package for ChIP peak annotation, comparison and visualization, Bioinformatics 31 (2015) 2382–2383.
[85] C. Perez-Llamas, Lopez-Bigas, N. Gitools, Analysis and visualisation of genomic data using interactive heat-maps, PLoS One 6 (2011), e19541.
[86] Y. Benjamini, D. Drai, G. Elmer, N. Kafkafi, I. Golani, Controlling the false discovery rate in behavior genetics research, Behav. Brain Res. 125 (2001) 279–284.
[87] A. Subramanian, et al., Gene set enrichment analysis: a knowledge-based approach for interpreting genome-wide expression profiles, Proc. Natl. Acad. Sci. U. S. A. 102 (2005) 15545–15550.
[88] V.K. Mootha, et al., PGC-1alpha-responsive genes involved in oxidative phosphorylation are coordinately downregulated in human diabetes, Nat. Genet. 34 (2003) 267–273.